An improved SPH model for multiphase flows with large density ratios

G.X. Zhu[a, b], L. Zou[a, b], Z. Chen[c], A.M. Wang[a, b], M.B. Liu[d,e *]

[a] *State Key Laboratory of Structural Analysis for Industrial Equipment, Dalian, 116024, China*

[b] *School of Naval Architecture, Dalian University of Technology, Dalian, 116024, China*

[c] *Department of Mechanical Engineering, National University of Singapore, 10 Kent Ridge Crescent, Singapore 119260, Singapore*

[d] *BIC-EAST, College of Engineering, Peking University, Beijing 100187, China*

[e] *State Key Laboratory for Turbulence and Complex Systems, Peking University, Beijing 100871, China*

Abstract

This paper presents a new SPH model for simuilating multiphase fluid flows with large density ratios. The new SPH model consists of an improved discretization scheme, an enhanced multiphase interface treatment algorithm and a coupled dynamic boundary treatment technique. The presented SPH discretization scheme is developed from Taylor series analysis with kernel normalization and kernel gradient correction, and is then used to discretize the Navier-Stokes equation to obtain improved SPH equations of motion for multiphase fluid flows. The multiphase interface treatment algorithm involves treating neighboring particles from different phases as virtual particles with specially updated density to maintain pressure consistency and a repulsive interface force between neighboring interface particles into the pressure gradient to keep sharp interface. The coupled dynamic boundary treatment technique includes a soft repulsive force between approaching fluid and solid particles while the information of virtual particles are approximated using the improved SPH discretization scheme. The presented SPH model is applied to three typical multiphase flow problems including dam breaking, Rayleigh-Taylor instability, and air bubble rising in

* Corresponding author. Tel.: +86-10-62766982

E-mail address: mbliu@pku.edu.cn (M.B. Liu)

This article has been accepted for publication and undergone full peer review but has not been through the copyediting, typesetting, pagination and proofreading process which may lead to differences between this version and the Version of Record. Please cite this article as doi: 10.1002/fld.4412

water. It is demonstrated that inherent multiphase flow physics can be well captured while the dynamic evolution of the complex multiphase interfaces are sharp with consistent pressure across the interfaces.

Keywords: Smoothed Particle Hydrodynamics, multiphase flows, interface, large density ratios

1 Introduction

Multiphase flows are common and important in engineering and science (e.g. oil recovery [1], carbon sequestration [2], drug delivery [3], sediment transport [4] and etc.). In multiphase flows, there exists interfaces with sharp discontinuity of density, viscosity and some other material properties. It is usually challenging to simulate multiphase flows due to this sharp material discontinuity. For example, for conventional Eulerian grid-based methods (finite difference method [5] and finite volume method [6]), special algorithms are required to treat or track the interface between different phases. Moreover, it is very difficult to analyze the details of the multiphase physics because of the lack of history and the smearing of information as the mass moves through the fixed-in-space Eulerian mesh. Lagrangian grid-based methods (such as the finite element method [7]) are capable of capturing multiphase interfaces and other moving features as the grid is attached on fluids/materials. However, for multiphase flows with rapid evolution of interfaces, the severely distorted mesh may result in very inefficient small time step, and may even lead to the breakdown of the computation.

Smoothed particle hydrodynamics (SPH) is a purely Lagrangian, meshfree particle method. SPH was originally invented by Gingold and Monaghan [8] and Lucy [9] to investigate astrophysical problems in three dimensional open space and lately it has been extended to many areas, especially for problems with large deformation and moving features. As a Lagrangian particle method, SPH conserves mass exactly. In SPH, there is no explicit interface tracking for multiphase flows—the motion of the fluid is represented by the motion of the particles, and fluid surfaces or fluid–fluid interfaces move with particles representing their phases defined at the initial stage. Therefore SPH seems attractive in modeling

multiphase flows. For example, In 1995, Monaghan [10] demonstrated the feasibility of modeling two phase flow with small density ratios with a conventional SPH formulation. Later, Colagrossi and Landrini [11] showed that using a conventional SPH formulation with weakly compressible fluid is not able to maintain a stable interface and is usually associated with large numerical oscillation around the interface, especially for multiphase flows with large density ratios (e.g., water-air flow with a typical density ratio of around 800).

In the conventional SPH methods, the multiphase interface with sharp material discontinuity is not properly treated. It is believed that this is the major reason why conventional SPH is not able to model multiphase flows with large density ratios. As such, various ways are proposed to modify the conventional SPH for modeling multiphase flows. For example, in 2003, Colagrossi and Landrini [11] presented some modifications including density re-initialization, artificial viscosity optimization, a cohesive force together with the XSPH technique on the conventional SPH method to model interfacial flows with large density ratios. Hu and Adams [12, 13] presented a multi-phase SPH method for macroscopic and mesoscopic flows and an incompressible multiphase SPH method. Later, Adami and Hu [14] proposed a weakly compressible multiphase SPH with a new surface-tension formulation. These multiphase SPH models, either based on incompressible or weakly compressible concept, have not been applied to problems with rapidly evolving complex interfaces or free surfaces. Grenier et al. [15] presented another multiphase SPH model, in which a shepard kernel was used to recover an accurate interpolation and a small artificial repulsive force was also introduced in their model to keep the interface sharp. In 2013, Monaghan and Rafiee [16] also proposed a simple SPH algorithm for multi-fluid flow. They found that it is necessary to employe a small increase in pressure for interactions between different fluids in order to keep interface stable. A two-phase SPH modeling with a sharp interface method is proposed by Zhang and Deng [17] . In their work, the level set function is introduced to capture the interface implicitly. Chen et al. [18] proposed a new SPH model for multiphase flows with complex interfaces and large density differences. This model considered pressure continuity over the interfaces and the particles from different phases are

treated the same phase particles, except for the density. Recently, a new two-phase incompressible-compressible SPH method was developed by Lind et al [19], in which the compressible phase provides a pressure boundary condition at the interface for the incompressible phase, while the incompressible phase provides a velocity boundary condition for the compressible phase.

In most existing multiphase SPH models, the conventional SPH approximation scheme is used, which has poor accuracy especially for highly disordered particle distribution. As such, some technuiqes to adapt particles to be more regular or even were presented, including XSPH [20] and PSA (particle shifting algorithm) [21, 22]. Some literature used modified approximation techniques for partial applications. For example, in Colagrossi and Landrini work [11], density re-initialization was used based on moving least squre. In Grenier's work [15], a shepard kernel is applied to enhance the unity in support domain near the interface. One good way is to improve the conventional SPH method systemtically with corrected or enhanced approximation schemes. During the last decade, different such approaches have been proposed to improve the particle inconsistency and hence systematically improve the SPH approximation accuracy. Some of them involve reconstruction of a new smoothing function so as to satisfy the discretized consistency conditions. One typical example is the reproduced kernel particle method (RKPM) proposed by Liu and his co-workers [23]. Recently, one popular way is to construct improved SPH approximation schemes based on Taylor series expansion on the SPH approximation of a function and its derivatives. Typical examples include the corrective smoothed particle method (CSPM) by Chen and Beraun [24] and the finite particle method (FPM) by Liu et al. [25]. Both CSPM and FPM do not need to reconstruct smoothing function. It was reported that CSPM and FPM have better accuracy and better ability than the conventional SPH method, while they need to re-structure the existing SPH code with more computational efforts. This is because, in the conventional SPH method, a field function and its derivatives are approximated separately. Instead, in CSPM, the derivatives are approximated through solving a coupled matrix equation while the field function is approximated separately. In FPM, both the field function and its derivatives are

coupled together and can be approximated simultaneously through solving a general matrix equation.

This paper follows the previous work by Chen el al [17] with an improved SPH approximation scheme when discretizing Navier-Stokes equations to obtain improved SPH equations of motion for multiphase fluid flows. An enhanced interface treatment algorithm is also provided to ensure numerical accuracy and stability around the multiphase interfaces. The effectiveness of the presented multiphase SPH model is then to validated with three typical multiphase flow problems including dam breaking, Rayleigh-Taylor instability, and air-bubble rising.

2 Governing Equations

The governing equations for the flow of an isothermal fluid can be written in a Lagrangian form as

$$\frac{d\rho}{dt} = -\rho\nabla\cdot\boldsymbol{u} \tag{1}$$

$$\frac{d\boldsymbol{u}}{dt} = -\frac{1}{\rho}\nabla P + \boldsymbol{F}_v + \boldsymbol{g} \tag{2}$$

where ρ, $\boldsymbol{u}$ and P denote the density, the velocity and the pressure, respectively. And $\boldsymbol{F}_v$ and $\boldsymbol{g}$ represent the viscous and the external body forces.

The viscous force $\boldsymbol{F}_v$ can be written as

$$\boldsymbol{F}_v = \nu\nabla^2\boldsymbol{u} \tag{3}$$

where υ is the kinematic viscosity.

When modeling incompressible flows, it is feasible to use the artificial compressibility concenpt which assumes the incompressible fluid to be weakly compressible. This artificial compressibility concept thus provide a simple way to compute pressure from the density of the fluid through an artificial equation of state and can greatly reduce the redundancy in pressure calculation especially in meshfree and particle methods including SPH and MPS (moving particle semi-impliclit method) [26-29]. In this paper, the following equation of state is applied

$$P = c_0^2(\rho - \rho_0) + P_0 \tag{4}$$

where c_0 is the numerical sound of speed, used to control the compressibility and to fulfill the incompressible limit. To ensure that the density oscillations is within 1% as to meet the hypothesis of weak compressibility, the numerical sound of speed should be 10 times or larger than the maximal fluid velocity [30]. P_0 is the background pressure. The purpose of introducing background pressure is to avoid negative particle pressure (which could threaten the computational stability) and to certain extent, model the expansion effect of the fluid.

3 Numerical model

3.1 Briefing on the conventional SPH method

In the basic SPH method [31], the fluid can de discretized into a set of partiles which carry mass, density, velocity and other physical properties. A function $A(\boldsymbol{r}_i)$ can be approximated at a nearby position $\boldsymbol{r}_j$ as following form

$$A(\boldsymbol{r}_i) = \sum_j A(\boldsymbol{r}_j) W(\boldsymbol{r}_{ij}) \Delta V_j \tag{5}$$

where the subscript j denotes the neighboring particles of particle i in thr support domain. While $\boldsymbol{r}$ is the position vector, $W(\boldsymbol{r}_{ij})$ is the kernel function. ΔV_j is the volume associated with particle *j*, and it can be replaced with the ratio of particle mass to density (i.e., $\Delta V_j = \frac{m_j}{\rho_j}$). According to Hongbin and Xin ' work [32], among 10 proposed kernels, the Gaussian function and the quantic function show better accuracy than others. Here the Gaussian kernel with a compact support of $3h$ is adopted

$$W(\boldsymbol{r}_{ij}) = \frac{1}{(\sqrt{\pi}h)^2} e^{-(s)^2} \tag{6}$$

where $s = (\boldsymbol{r}_i - \boldsymbol{r}_j)/h$.

The spatial derivatives $\nabla A(\boldsymbol{r}_i)$ of the function can be similarly written as

$$\nabla A(\boldsymbol{r}_i) = \sum_j A(\boldsymbol{r}_j) \nabla W(\boldsymbol{r}_{ij}) \Delta V_j \tag{7}$$

where ∇ denotes the derivative with respect to $\boldsymbol{r}$.

3.2 Improved SPH approximations

Though the conventional SPH method has been widely applided to different areas in

engineering and sceinces, it is often referred to a as a low order computational method since it cannot exactly reproduce quadratic and linear functions, and even cannot exactly reproduce a constant, especially when particles are irregularly distributed [31]. During last decades, many modified SPH approximation techniques have been proposed to improve the accuracy of the convetional SPH method while most of them need to siginificantly modify the structure of existing SPH code with considerable burden. Here, we give a general way to correct the SPH approximation of a function and its derivatives.

Numerical simulations usually involve approximation of the values of a function and its derivatives at a certain point. Performing Taylor series expansion at a nearby point $\boldsymbol{r}_i$ and retaining up to the first order derivatives, a sufficiently smooth function $A(\boldsymbol{r}_j)$ at the point $\boldsymbol{r}_j$ can be expressed as

$$A(\boldsymbol{r}_j) = A(\boldsymbol{r}_i) + \nabla A(\boldsymbol{r}_i) \cdot (\boldsymbol{r}_j - \boldsymbol{r}_i) + \mathcal{O}(h^2) \tag{8}$$

If the terms involving derivatives in this equation are neglected (ignoring 1st order derivatives), multiplying both sides of the Eq. (8) by the smoothing function $W(\boldsymbol{r}_{ij})$ and intergrating over the entire computational domain yield

$$\int A(\boldsymbol{r}_j) W(\boldsymbol{r}_{ij}) d\boldsymbol{r} = A(\boldsymbol{r}_i) \int W(\boldsymbol{r}_{ij}) d\boldsymbol{r} \tag{9}$$

Then, a corrective kernel approximation for function $A(\boldsymbol{r}_i)$ at particle i is obtained as

$$A(\boldsymbol{r}_i) = \frac{\int A(\boldsymbol{r}_j) W(\boldsymbol{r}_{ij}) d\boldsymbol{r}}{\int W(\boldsymbol{r}_{ij}) d\boldsymbol{r}} \tag{10}$$

Using summation over nearest particles for each term in Eq. (10), the corresponding particle approximation for function $A(\boldsymbol{r}_i)$ at particle i position can be obtained

$$A(\boldsymbol{r}_i) = \frac{\sum_j A(\boldsymbol{r}_j) W(\boldsymbol{r}_{ij}) \Delta V_j}{\Gamma} \tag{11}$$

where

$$\Gamma = \sum_j W(\boldsymbol{r}_{ij}) \Delta V_j \tag{12}$$

Similarly, multiplying both sides of the Eq. (8) with $\nabla W(\boldsymbol{r}_{ij})$ and integrating over the

entire computational domain yield

$$\int A(\boldsymbol{r}_j)\nabla W(\boldsymbol{r}_{ij})d\boldsymbol{r} = A(\boldsymbol{r}_i)\int \nabla W(\boldsymbol{r}_{ij})d\boldsymbol{r} + \int \nabla A(\boldsymbol{r}_i)\cdot(\boldsymbol{r}_j - \boldsymbol{r}_i)\nabla W(\boldsymbol{r}_{ij})d\boldsymbol{r} \tag{13}$$

For a conventional smoothing function (non-negative and symmetric), the first term at the right side of Eq. (13) is zero in the interior region. For boundary areas where the integration is truncated, it is possible to remedy the boundary difficiency by using ghost or virtual areas (with ghost or virtual particles when discretized). Therefore it is safe to assume

$$\int \nabla W(\boldsymbol{r}_{ij})d\boldsymbol{r} \cong 0 \tag{14}$$

Then we can get

$$\int A(\boldsymbol{r}_j)\nabla W(\boldsymbol{r}_{ij})d\boldsymbol{r} = \nabla A(\boldsymbol{r}_i)\int(\boldsymbol{r}_j - \boldsymbol{r}_i)\nabla W(\boldsymbol{r}_{ij})d\boldsymbol{r} \tag{15}$$

It is seen that for multi-dimensional problems, $\nabla A(\boldsymbol{r}_i)$ are actually coupled together with a set of equations multiplied by the kernel gradient at different directions. For example, in two dimentional questions, the particle approximation in the above SPH formulation can easily be written as

$$\begin{cases} \sum_j A(\boldsymbol{r}_j)\frac{\partial W_{ij}}{\partial x_i}\Delta V_j = \frac{\partial A(\boldsymbol{r}_i)}{\partial x_i}\sum_j x_{ji}\frac{\partial W_{ij}}{\partial x_i}\Delta V_j + \frac{\partial A(\boldsymbol{r}_i)}{\partial y_i}\sum_j y_{ji}\frac{\partial W_{ij}}{\partial x_i}\Delta V_j \\ \sum_j A(\boldsymbol{r}_j)\frac{\partial W_{ij}}{\partial y_i}\Delta V_j = \frac{\partial A(\boldsymbol{r}_i)}{\partial x_i}\sum_j x_{ji}\frac{\partial W_{ij}}{\partial y_i}\Delta V_j + \frac{\partial A(\boldsymbol{r}_i)}{\partial y_i}\sum_j y_{ji}\frac{\partial W_{ij}}{y_i}\Delta V_j \end{cases} \tag{16}$$

where $x_{ji} = x_j - x_i,\ y_{ji} = y_j - y_j$. The above equations can be rewritten in the form of matrix equation as

$$\boldsymbol{M}\begin{pmatrix} \frac{\partial A(\boldsymbol{r}_i)}{\partial x_i} \\ \frac{\partial A(\boldsymbol{r}_i)}{\partial y_i} \end{pmatrix} = \begin{pmatrix} \sum_j A(\boldsymbol{r}_j)\frac{\partial W_{ij}}{\partial x_i}\Delta V_j \\ \sum_j A(\boldsymbol{r}_j)\frac{\partial W_{ij}}{\partial y_i}\Delta V_j \end{pmatrix} \tag{17}$$

where

$$\boldsymbol{M} = \begin{pmatrix} \sum_j x_{ji}\frac{\partial W_{ij}}{\partial x_i}\Delta V_j & \sum_j y_{ji}\frac{\partial W_{ij}}{\partial x_i}\Delta V_j \\ \sum_j x_{ji}\frac{\partial W_{ij}}{\partial y_i}\Delta V_j & \sum_j y_{ji}\frac{\partial W_{ij}}{y_i}\Delta V_j \end{pmatrix} \tag{18}$$

By solving the matrix equation expressed in Eq. (17), the first order derivative $\nabla A(\boldsymbol{r}_i)$

of the function at particle i can be expressed as:

$$\begin{pmatrix} \frac{\partial A(\boldsymbol{r}_i)}{\partial x_i} \\ \frac{\partial A(\boldsymbol{r}_i)}{\partial y_i} \end{pmatrix} = \sum_{\boldsymbol{j}} A(\boldsymbol{r}_j)\Delta V_j \left(\boldsymbol{M}^{-1} \begin{pmatrix} \frac{\partial W_{ij}}{\partial x_i} \\ \frac{\partial W_{ij}}{\partial y_i} \end{pmatrix} \right) \tag{19}$$

It is shown that the above equation introduces a corrective maxtrix $\boldsymbol{M}$ when approximating the derivatives (in the conventional SPH method) . It is can be further regarded as the correction on the conventional kernel gradient $\nabla W_{ij}(\boldsymbol{r})$ as

$$\frac{\nabla W(\boldsymbol{r}_{ij})}{\boldsymbol{\mathcal{L}}} = \boldsymbol{M}^{-1}\nabla W(\boldsymbol{r}_{ij}) \tag{20}$$

It is noted that Eq. (12) is actually similar to that in CSPM when approximating a field function [24]. However, Eq. (20) is different from that in CSPH when approximating the derivatives of a field function and it involves kernel gradient correction (KGC). One advantage of this kernel gradient correction is that there is no need to significantly change the structure of existing SPH programs and procedure of SPH simulations since only the gradients of the smoothing kernel (or kernel gradients) are corrected [41].

3.3 The discretization of governing equations

In this paper, the velocity gradient is calculated using anti-symmetric form, as suggested by Monaghan and Rafiee when modelin multi-fluids [16]. Considering the kernel graddient correction as described in Section 3.2, hence the improved SPH discretization of the continuity equation is expressed as:

$$\frac{d\rho_i}{dt} = \frac{1}{\rho_i}\sum_j \Delta V_j(\boldsymbol{u}_i - \boldsymbol{u}_j) \cdot \frac{\nabla W(\boldsymbol{r}_{ij})}{\boldsymbol{\mathcal{L}}} \tag{21}$$

According to the discussion in Section 3.2, the SPH discretization of the momentum equation can be rewritten as

$$\frac{d\boldsymbol{u}_i}{dt} = \frac{1}{\rho_j}\sum_j P_j \Delta V_j \cdot \frac{\nabla W(\boldsymbol{r}_{ij})}{\boldsymbol{\mathcal{L}}} + \boldsymbol{F}_{ij}^{v} + \boldsymbol{g} \tag{22}$$

Following the work by Hu and Adams [12], the viscous force can be written as after kernel gradient correction

$$\boldsymbol{F}_{ij}^{v} = \sum_j \frac{2\nu_i\nu_j}{\nu_i+\nu_j} \frac{(\boldsymbol{x}_i-\boldsymbol{x}_j)\cdot(\boldsymbol{u}_i-\boldsymbol{u}_j)}{r_{ij}^2} \frac{\nabla W(\boldsymbol{r}_{ij})}{\boldsymbol{\mathcal{L}}} \Delta V_j \tag{23}$$

where $r_{ij} = |\boldsymbol{r}_j - \boldsymbol{r}_i|$.

3.4 The multiphase interface treatment

The treatment of interface between different materials, fluids and phases are very important for problems with multi-materials, multi-fluids and multi-phases. Improper treatment of interface may result in numerical oscillations in the interface area and may also cause unphysical particle penetration. Many works generally consider the contribution of particles from different materials when conducting particle approximations. This is a flexible but rough implementation of the interface condition (equal velocity and equal stress acros the interface), and is not suitable for problems with large density ratio (e.g., bubble rising with a water-air ratio of nearly 1000).

In this work, a new interface treatment algorithm is developed for modeling multiphase flows with large density ratios. The new interface treatment algorithm consists of two techniques, *a virtual particle technique* and *an interface force*. In the virtual particle technique, neighboring particles from different phases are used as virtual particles for each phase when modeling multiphase interface. It is noted that over the interface, pressure should be continuous. As such, when conducting SPH particle approximations with contribution of particles from different phase, position, volume, velocity and pressure of neighboring virtual particles are directly used. Instead, it is not suitable to directly use particle density from neighboring virtual particle as this can cause large numerical oscillation for multiphase flows with large density ratio. The density of a neighboring virtual particle needs to be carefully calculated to enforce pressure consistency over the interface.

Thus, considering a density field approximated by Eq. (11)

$$\rho_i = \sum_j \rho_j \frac{W(\boldsymbol{r}_{ij})}{\Gamma} \Delta V_j \tag{24}$$

Specially, Eq. (24) can produce a large numerical oscillation as the discontinuous density, when the support domain is close to the multiphase interface. According to the concept of pressure continuity as suggested by Chen et al [18], when approximating the density of a particle near the multiplase interface, Eq. (24) can be written as

$$\rho_i = \sum_{j\in S} \rho_j \frac{W(\boldsymbol{r}_{ij})}{\Gamma} \Delta V_j + \sum_{j\in D} \rho_j^* \frac{W(\boldsymbol{r}_{ij})}{\Gamma} \Delta V_j \tag{25}$$

where subscript S denotes a neighboring particle j in the *same* phase as particle i, subscript D denotes a neighboring particle j in the phase *different* from particles i. ρ_j^* is the density obtained by the pressure of particle j and the equation of state for particle i. And the density ρ_j^* can be obtained by the following form

$$\rho_j^* = \frac{P_j - P_0}{c_{j0}^2} + \rho_{j0} \tag{26}$$

where ρ_{j0} denotes the reference density of particle j and c_{j0} denotes the reference numerical sound of speed. Thus, the density of the paricles near the interface can be obtain by Eq. (25). Actually, Eq. (25) has the same expression with density re-initialization and every 10 time steps is applied in this paper.

In the new interface treatment algorithm, in order to keep the interface sharp, a small repulsive interface force [42] is introduced in the pressure gradient

$$\nabla P_i = \sum_j P_j \Delta V_j \cdot \frac{\nabla W(\boldsymbol{r}_{ij})}{\boldsymbol{\mathcal{L}}} + \epsilon \sum_{j\epsilon \boldsymbol{\mathcal{D}}} P_j \Delta V_j \frac{\nabla W(\boldsymbol{r}_{ij})}{\boldsymbol{\mathcal{L}}} \tag{27}$$

where ϵ is the interface force coefficient ranging 0.01 and 0.1 following Grenier's suggestion [15]. The first summation applies to the all particles in the support domain and the second summation applies to neighboring particles in the phase different from particles (marked by $\boldsymbol{\mathcal{D}}$).

3.5 Coupled dynamic solid boundary treatment

Boundary condition is an important issue in SPH method, and accurate implementation of boundary conditions is still a challenge. There are different treatments for solid boundaries in SPH. The repulsive boundary treatment method [26] and the dynamic boundary treatment method [33] are two frequently used solid boundary models. The repulsive boundary treatment is simple and adaptive to complex solid boundary. However, since there are no sufficient neighbor particles for a fluid particle in the support domain, the numerical accuracy is usually poor. In dynamic boundary treatment, virtual particles are placed in the boundary. Thus, this treatment may have better accuracy by removing the particle deficiency. However, fluid particles may unphysically penetrate the solid walls in many cases.

In this paper, the coupled dynamic solid boundary treatment algorithm, developed originally by Liu et al. [34] and later further modified by Chen et al. [35] is applied in following simulations of multiphase flows. One layer of repulsive particles are deployed right on the solid boundary and two other layers of ghost particles are located in outer boundary areas. The ghost particles are treated as denser fluid particles. All the ghost particles are statically fixed on the solid boundary without velocity. The density of these particles is obtained through Eq. (25). When a fluid particle approaches the solid wall, the following repulsive force is applied between the repulsive particles and the fluid particle to prevent unphysical particle penetration

$$\boldsymbol{F}_{ij} = 0.01c_0^2 \cdot \chi \cdot f(\alpha) \cdot \frac{\boldsymbol{r}_{ij}}{|\boldsymbol{r}_{ij}|^2} \cdot m_{fluid} \tag{28}$$

$$\chi = \begin{cases} 1 - \frac{|\boldsymbol{r}_{ij}|}{h}, & 0 < |\boldsymbol{r}_{ij}| < h \\ 0, & otherwise \end{cases} \tag{29}$$

$$\alpha = \frac{|\boldsymbol{r}_{ij}|}{0.5h} \tag{30}$$

$$f(\alpha) = \begin{cases} 2/3, & 0 < \alpha < 2/3 \\ (2\alpha - 1.5\alpha^2), & 2/3 < \alpha < 1 \\ 0.5(2-\alpha)^2, & 1 < \alpha < 2 \\ 0, & otherwise \end{cases} \tag{31}$$

where m_{fluid} is the mass of the approaching fluid particle.

3.6 Time-stepping scheme

In present simulation, a prediction-correction time-stepping scheme is applied to ensure second order accuracy [20]. The scheme obtains two steps.

1. The prediction step:

$$\begin{cases} \boldsymbol{u}_i^{n+\frac{1}{2}} = \boldsymbol{u}_i^n + \frac{\Delta t}{2}\left(\frac{d\boldsymbol{u}}{dt}\right)_i^n \\ \rho_i^{n+\frac{1}{2}} = \rho_i^n + \frac{\Delta t}{2}\left(\frac{d\rho}{dt}\right)_i^n \\ \boldsymbol{r}_i^{n+\frac{1}{2}} = \boldsymbol{r}_i^n + \frac{\Delta t}{2}\boldsymbol{u}_i^n \end{cases} \tag{32}$$

where the superscript n denotes number of the time step, Δt denotes the time step.

2. The correction step:

$$\begin{cases} \boldsymbol{u}_i^{n+1} = \boldsymbol{u}_i^{n+\frac{1}{2}} + \frac{\Delta t}{2}\left(\frac{d\boldsymbol{u}}{dt}\right)_i^{n+\frac{1}{2}} \\ \rho_i^{n+1} = \rho_i^{n+\frac{1}{2}} + \frac{\Delta t}{2}\left(\frac{d\rho}{dt}\right)_i^{n+\frac{1}{2}} \\ \boldsymbol{r}_i^{n+1} = \boldsymbol{r}_i^{n+\frac{1}{2}} + \frac{\Delta t}{2}\boldsymbol{u}_i^{n+\frac{1}{2}} \end{cases} \tag{33}$$

Therefore after one time step, the variables of each particles are updated as

$$\begin{cases} \boldsymbol{u}_i^{n+1} = 2\boldsymbol{u}_i^{n+\frac{1}{2}} - \boldsymbol{u}_i^n \\ \rho_i^{n+1} = 2\rho_i^{n+\frac{1}{2}} - \rho_i^n \\ \boldsymbol{r}_i^{n+1} = \boldsymbol{r}_i^{n+\frac{1}{2}} - \boldsymbol{r}_i^n \end{cases} \tag{34}$$

Moreover, in order to ensure the numerical stability, the maximum time-step is chosen based on several criteria [36, 37]. Here, the time step must be constrained by Courant-Friedrichs-Lewy (CFL) condition based on the artificial sound speed c_0:

$$\Delta \mathrm{t} \leq \frac{h}{c_0} \tag{35}$$

the viscous diffusion condition:

$$\Delta \mathrm{t} \leq 0.125\frac{h^2}{\upsilon} \tag{36}$$

and the body force condition:

$$\Delta \mathrm{t} \leq 0.25\sqrt{\frac{h}{g}} \tag{37}$$

For satisfying all conditions the global time-step is taken as minimum of Eqs. (35)-(37).

4 Numerical Examples

4.1 Dam breaking

The dam breaking problem is a typical benchmark for testing free surface or multiphase flows as comprehensive analytical, numerical and experimenta data are available for the validation of new numerical models. Here we consider air-water two phases with a water to air density ratio of around 800. The width and the height of computational domain are $1.6\,m$ and $0.5\,m$, as shown in Fig. 1. The initial size of water column with the reference density of $1000\ kg/m^3$ is $0.6\,m \times 0.3\,m$. While air with the reference density of $1.29\ kg/m^3$ is at

rest in the rectangular computational domain. The initial particle spacing is chosen as $0.005\ m$, and approximately 34000 particles are used in simulations. Time step is set to be $2.5 \times 10^{-6}\ s$. The background pressure is 2000 Pa.

Fig. 2 shows the particle distribution and pressure contour of the dam breaking process at $t\sqrt{g/h} = 3.2$ and $t\sqrt{g/h} = 6.4$, respectively. It is seen that physics inherent in dam breaking including wave front and water height can be well captured. The obtained pressure field is smooth and the water-air interface is sharp and stable. More flow details such as the impacting of water wave on front wall, splashing back and forming water jet can also be well described.

Fig. 3 shows the pressure history (non-dimensional) of a pressure observation point located at 0.06 m from the bottom of the right wall. Results from present SPH simulation are compared with the experimental data [38] and results from Colagrossi et al [11]. It is seen that the pressure history curves from three approaches in general are agreeable. Before $t\sqrt{g/h} = 2.5$, as the water front has not arrived, the pressure on the observation point is acutally zero. At $t\sqrt{g/h} = 2.5$, when water wave arrives and impacts on the right solid wall, pressure on the observation point suddently increases as a shock wave. After then, the impact-induced pressure load on the observation point gradually reduces and approaches a roughly constant pressure as water continuously moves along the right solid wall. Later some water particles splash back and plunge into the bulky water due to the interaction of gravitiy and momental inertia, as shown in Fig. 2. This will form a water jet from the bulky water and generate second water wave. This new water wave propogats towards the right solid wall and will produceds a second pressure shock on the pressure observation point at around $t\sqrt{g/h} = 6.0$, followed by similar decay process. As shown in Fig. 3, the presented SPH

model captures inherent complex physics in water impact while the position (non-dimensional instants) and correspoinding magnitude of the first pressure shock agree very well with those from experimental observation. The second pressure shock is associated with a slightly smaller magnitude at a later time stage than the experimental observation. It is interesting that in Colagrossi et al' work, after $t\sqrt{g/h} = 2.5$, water pressure gradually increases to become roughly constant. This is different from real physics with a sudden increase to a peak shock pressure followed by gradual decay, as seen in the present SPH and experimental results.

4.2 Rayleigh-Taylor instability

Here, we consider the Rayleigh-Taylor instability problem which was also studied by some other researchers including Hu et al. [13]; Grenier et al. [15]; Monaghan and Rafiee [16] and Chen et al [18] using different versions of SPH method. In this problem, the computation domain is a $1\,m \times 2\,m$ rectangle container with a heavier fluid placed on a lighter fluid, as shown in Fig .4. The heavier fluid is marked using green color with the density of $1800\ kg/m^3$ and the lighter fluid is marked blue color with the density of $1000\ kg/m^3$. The two fluids are separated by an interface perturbed according to $y = 1.0 - 0.15\,sin(2\pi x)$. The gravity acceleration is $g = 1\ m/s^2$. The initial time stepping is $1 \times 10^{-5}\,s$. The initial particle space is 0.01m and the number of particles is 40000 (100×200 along x and y direction). The background pressure is 100 Pa.

Fig. 5 shows the particle positions and the pressure contour of our simulation at $\mathrm{t} = 1$ s, $3\,s$ and $5\,s$. It is seen that the density difference between the heavy and light fluids leads to instability and this two fluid system starts to evolve due to gravity and generates complex fluid interface. The evolution of the fluid interface is well captured and the pressure field around the interface area is also smooth.

Fig. 6 shows the time history of the highest point of the light fluid is presented together with the theoretical results from Dalziel's work [39]. Three cases with different number of

particles, 50×100, 100×200 and 200×400, are simulated. It is shown that with more than 50×100 particles, increasing the total number of particles does not significantly change the simulation results. This means that the obtained simulation results arrive at a convergent solution, which is close to the theoretical solution from Dalziel's work [39]. It's found that the Grenier's results about highest point of the lighter fluid at $5\,s$ deviates from the theoretical solution. This quantitatively proves that our method is more accurate. Due to the interface force in the present SPH model, the obtained fluid interface is much sharper than that in Chen et al.'s work [18] , in which some particles from the lighter fluid unphysically penetrate the heavier fluid and this leads to a comparatively vaguer fluid interface, as shown in Fig. 7a.

4.3 Air bubble rising in water

This example involves the rising of an air bubble in water, which was also modeled by Sussman et al. [40] using the Level-Set algorithm to track the fluid interface. In this example, the radius of the bubble is $R = 0.1\,m$. The width and height of the tank are $6R$ and $10R$, as shown in Fig. 8. The problem involves a density ratio of 1000 (water density $1000\ kg/m^3$ and air density $1.0\ kg/m^3$) and a kinematic viscosity ratio of 200. The initial time stepping is $2.5 \times 10^{-6}\,s$. The parameter ϵ in the interface force is set to 0.08. The initial particle space is $0.0025\,m$ and with a total number of 480,000 particles (240×400 along x and y direction). The background pressure is 1000 Pa.

Fig. 9 shows the simulated bubble shape evolution process at 9 sequencing instants as it raises in water (water particles are not plotted). It is seen that the present SPH model can well capture the water-air interface. As time passes, the upwelling water motion deforms the bubble which attains a horseshoe shape. Then the jet broadens, the tips of the bubble roll up and smaller bubbles are eventually detached. The water-air interface from Level-Set simulation are also provided for comparison. In general, the present SPH results are in good agreement with Level-Set results. Due to different nature (particle-based vs grid-based) of

these two approaches, some discrepancies exist. For example, before $t\sqrt{g/h} = 4.4$ while the bubble nearly pinches off, the thickness of the bubble from present SPH simulation is slightly smaller than that in Level-Set simulation. At $t\sqrt{g/h} = 4.8$, and the Level-Set simulation predicts four bubbles (two larger bubbles and two smaller next to the two major bubbles), while the present SPH simulation only predicts only larger bubbles which are close to the two larger bubbles in Level-Set simulation. The smaller bubbles in the Level-Set simulation disappear at $t\sqrt{g/h} = 5.6$ while another small bubble appear at $t = \sqrt{g/h} = 5.6$. The bubble rising problem was also investigated by Colagrossi and Landrini [11] using SPH method and they found the same discrepancies between SPH and Level-Set results.

The presented numerical example is in the scale of meter. Surface tension effects at such scale are negligible. However, when scale reduces to micro-meter and even smaller, the surface tension effects can be quite important. In SPH, it is easy and straightforward to include surface tension models, either using the continuum surface force model (CSF) [14,43,44]or the inter-particle interaction force (IIF) model [45].

Fig. 10 shows the pressure field at $t\sqrt{g/h} = 3.0$. Again the obtained pressure field is smooth and the water-air interface with horseshoe shape is sharply captured.

Fig. 11 shows SPH simulation at $t\sqrt{g/h} = 2.8$ with different initial particle space ranging from $0.005\,m$, $0.0025\,m$ to $0.00125\,m$. It is seen that after the initial particle space is smaller than $0.0025\,m$, increasing the total number of particles does not significantly change the simulation results. This means that the obtained simulation results arrive at a convergent solution. This demonstrate that the present SPH model is robust and has good convergent performance.

5 Conclusion

This paper presents an improved SPH model for multiphase flows with large density ratios and complex interfaces. Major improvements include a corrective SPH discretization

scheme and an enhanced multiphase interface treatment algorithm. The corrective SPH discretization scheme is from Taylor series analysis with kernel normalization and kernel gradient correction and is straightforward to use without significant modification on the structure of existing SPH programs and procedure of SPH simulations since only the kernel gradients are corrected. When treating multiphase interface, neighboring particles from different phase are regarded as virtual particles with specially updated density to ensure pressure consistency around the interface. A soft repulsive force is applied to neighboring interface particles into the pressure gradient to keep sharp interface. Three typical multiphase flow problems including dam breaking, Rayleigh-Taylor instability, and air-bubble rising are simulated using the improved SPH model while simulation results are compared with those from other sources. It can be concluded that the improved SPH model can well model multiphase flows with large density ratios. The multiphase interface can be sharply captured and the obtained pressure field is smooth across the interface area.

Acknowledgement

The present work is supported by 973 program(2013CB036101), the National Natural Science Foundation of China (Grant Nos 51379033, 51522902, 51579040, 11172306 and U1530110), the Fundamental Research Funds for the Central Universities（DUT15LK43, DUT15LK30）.

References

1. Paul EL, Atiemo OV, Kresta SM. *Handbook of Industrial Mixing: Science and Practice*, John Wiley & Sons, New Jersey, 2004.
2. Liu MB, Meakin P, Huang H. Dissipative particle dynamics simulation of pore-scale multiphase fluid flow. *Water Resources Research* 2007; 43: 244-247.
3. Liu MB, Chang JZ, Li HQ. Numerical modeling of injection flow of drug agents for controlled drug delivery, in: 29th Annual International Conference of the IEEE. Engineering in Medicine and Biology Society, EMBS 2007, 2007; 1152-1155.
4. James SC, Jones CA, Grace MD, Roberts JD. Advances in sediment transport modelling. *Journal of Hydraulic Research* 2010; 48: 754-763.
5. Mitchell AR, Griffiths DF. *The Finite Difference Method in Partial Differential Equations*, John Wiley, New York, 1980.
6. Versteeg HK, Malalasekera M. *An Introduction to Computational Fluid Dynamics: The Finite Volume*

Method, Pearson Education, Essex, 2007.

7. Idelsohn SR, Onate E, Pin DE. The particle finite element method: a powerful tool to solve incompressible flows with free-surfaces and breaking waves. *International Journal Numerical Methods in Engineering* 2004; 61: 964-989.
8. Gingold RA, Monaghan JJ. Smooth Particle Hydrodynamics: theory and application to non spherical stars. *Monthly Nottices of the Royal of Astronomical Society* 1977; 181: 375-389.
9. Lucy LB. A numerical approach to the testing of the fission hypothesis. *Astronomical Journal* 1977; 82: 1013-1024.
10. Monaghan JJ, Kocharyan A. SPH simulation of multi-phase flow. *Computer Physics Communication* 1995; 87: 225-235.
11. Colagrossi A, Landrini M. Numerical simulation of interfacial flows by smoothed particle hydrodynamics. *Journal of Computational Physics* 2003; 191: 448-475.
12. Hu XY, Adams N. A multi-phase SPH method for macroscopic and mesoscopic flows. *Journal of Computational Physics* 2006; 213: 844-861.
13. Hu XY, Adams N. An incompressible multi-phase SPH method. *Journal of Computational Physics* 2007; 227: 264-278.
14. Adami S, Hu XY, Adams N. A new surface-tension formulation for multi-phase SPH using a reproducing divergence approximation. *Journal of Computational Physics* 2009; 229: 5011-5021.
15. Grenier N, Antuono M, Colagrossi A, Touzé DL, Alessandrini B. An Hamiltonian interface SPH formulation for multi-fluid and free surface flows. *Journal of Computational Physics* 2009; 228: 8380-8393.
16. Monaghan JJ, Rafiee A. A simple SPH algorithm for multi-fluid flow with high density ratios. *International Journal for Numerical Methods in Fluids* 2013; 71: 537-561.
17. Zhang MY, Deng XL. A sharp interface method for SPH. *Journal of Computational Physics* 2015; 302: 469-484.
18. Chen Z, Zong Z, Liu MB, Zou L, Li HT, Shu C. An SPH model for multiphase flows with complex interfaces and large density differences. *Journal of Computational Physics* 2015; 283: 169-188.
19. Lind SJ, Stansby PK, Rogers BD. Incompressible-compressible flows with a transient discontinuous interface using smoothed particle hydrodynamics (SPH). *Journal of Computational Physics* 2016; 309: 129-147.
20. Monaghan JJ. On the problem of penetration in particle methods. *Journal of Computational Physics* 1989;82: 1-15.
21. Lind SJ, Xu R, Stansby PK, Rogers BD. Incompressible smoothed particle hydrodynamics for free-surface flows: A generalised diffusion-based algorithm for stability and validations for impulsive flows and propagating waves. *Journal of Computational Physics* 2012; 231: 1499-1523.
22. Xu R, Stansby PK, Laurence D. Accuracy and stability in incompressible SPH (ISPH) based on the projection method and a new approach. *Journal of Computational Physics* 2009; 228: 6703-6725.
23. Liu WK, Chen Y, Jun S, Chen JS, Belytschko T, Pan C, Uras RA, Chang CT. Overview and Applications of the Reproducing Kernel Particle Methods. *Archives of Computational Methods in Engineering* 1996; 3: 3-80.
24. Chen JK, Beraun JE. A generalized smoothed particle hydrodynamics method for nonlinear dynamic problems. *Computer Methods in Applied Mechanics and Engineering* 2000; 190: 225-239.

25. Liu MB, Xie WP, Liu GR. Modeling incompressible flows using a finite particle method. *Applied Mathamatics Modelling* 2009; 29: 1252-1270.
26. Monaghan JJ. Simulating free surface flows with sph. *Journal of Computational Physics* 1994; 110: 399-406.
27. Liu MB, Li S. On the modeling of viscous incompressible flows with smoothed particle hydro-dynamics. *Journal of Hydrodynamics Ser. B* 2006; 28: 731-745.
28. Koshizuka S, Nobe A, Oka Y. Numerical analysis of breaking waves using the moving particle semi-implicit method. *International Journal for Numerical Methods in Fluids* 1998; 26: 751-769.
29. Long T, Hu D, Yang G, Wan D. A particle-element contact algorithm incorporated into the coupling methods of FEM-ISPH and FEM-WCSPH for FSI problems. *Ocean Engineering* 2016; 123: 154-163.
30. Morris JP, Fox PJ, Zhu Y. Modeling low reynolds number incompressible flows using SPH. *Journal of Computational Physics* 1997; 136: 214-226.
31. Liu GR, Liu MB. *Smoothed Particle Hydrodynamics: A Meshfree Particle Method*, World Scientific, Singapore, 2003.
32. Jin HB, X. Ding X. On criterions for smoothed particle hydrodynamics kernels in stable field. *Journal of Computational Physics* 2005; 202: 699-709.
33. Gomez-Gesteira M, Darymple R. Using a three-dimensional smoothed particle hydrodynamics method for wave impact on a tall structure. *Journal of Waterway Port Coastal & Ocean Engineering* 2004; 130: 63-69.
34. Liu MB, Shao JR, Chang JZ. On the treatment of solid boundary in smoothed particle hydrodynamics. *Science China Technological Sciences* 2012; 55: 244-254.
35. Chen Z, Zong Z, Liu MB, Li HT. A comparative study of truly incompressible and weakly compressible SPH methods for free surface incompressible flows. *International Journal for Numerical Methods in Fluids* 2013; 73: 813-829.
36. Zhu Y, Fox PJ. Smoothed Particle Hydrodynamics Model for Diffusion through Porous Media, Trans. *Porous Media* 2001; 43: 441-471.
37. Monaghan JJ. Smoothed particle hydrodynamics. *Report Progress of Physics* 2005; 68: 1703-1759.
38. Zhou ZQ, Kat J, Buchner B. A nonlinear 3-D approach to simulate green water dynamics on deck, in: J. Piquet (Ed.), Proc. 7th Int. Conf. Num. Ship Hydrod, Nantes, 1999, pp. 5.1-1.
39. Dalziel S. Toy models for Rayleigh Taylor instability. 8th International Workshop on the Physics of Compressible Turbulent Mixing, Lawrence Livermore National Laboratory, UCRL-MI-146350, 2001.
40. Sussman M, Smereka P, Osher S. A level set approach for computing solutions to incompressible two-phase flow. *Journal of Computational Physics* 1994; 114: 146-159.
41. Shao JR, Liu MB, Yang XF, Cheng L. Improved smoothed particle hydrodynamics with RANS for free surface flow problems. *International journal of computational methods* 2012; 9: 367-374.
42. Yang XF, Liu MB. Numerical modeling of oil spill containment by boom using SPH. *Science China Physics, Mechanics and Astronomy* 2013; 56: 315-321.
43. Zhang M. Simulation of surface tension in 2D and 3D with smoothed particle hydrodynamics method. *Journal of Computational Physics* 2010; 229: 7238-7259.
44. Zhang M, Deng XL. A sharp interface method for SPH. *Journal of Computational Physics* 2015; 302: 469-484.
45. Liu MB, Liu GR. Smoothed Particle Hydrodynamics (SPH): an Overview and Recent Developments. *Archives of Computational Methods in Engineering* 2010; 17: 25-76.

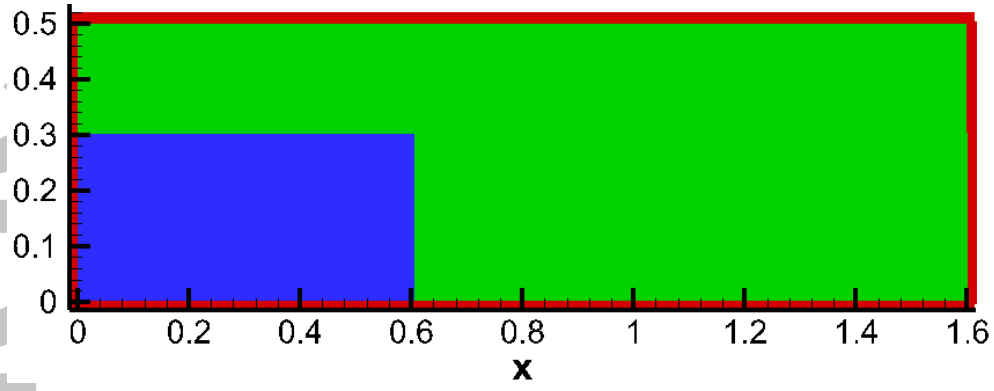

Fig. 1. Initial set up of dam breaking. The air and water phase are green and blue, respectively.

(a)

(b)

(c)

(d)

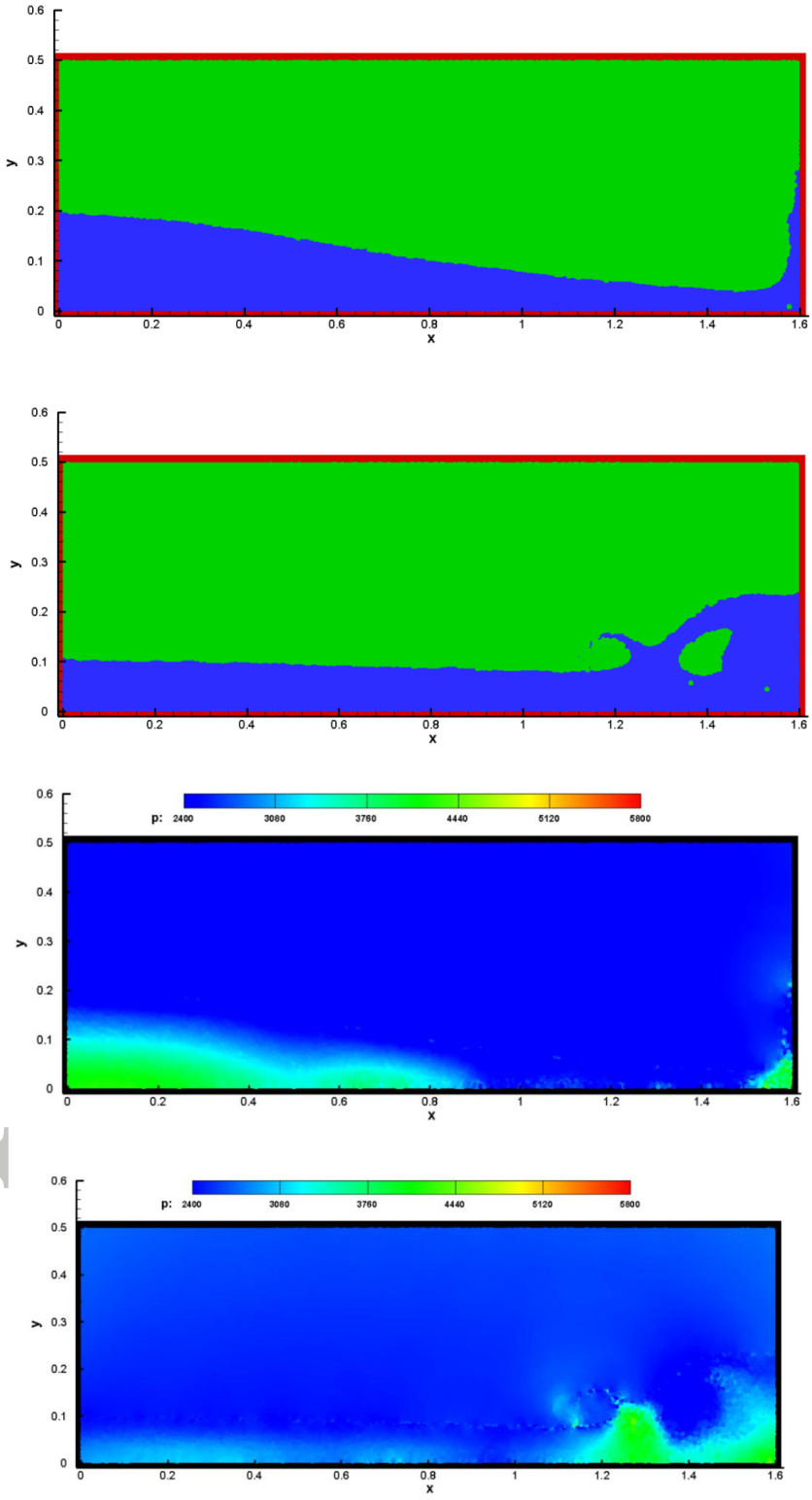

Fig. 2. Simulation snapshot at different instants. (a) Phase distribution at $t\sqrt{g/h} = 3.2$; (b) Phase distribution at $t\sqrt{g/h} = 6.4$; (c) Pressure contour at $t\sqrt{g/h} = 3.2$; (d) Pressure contour at $t\sqrt{g/h} = 6.4$.

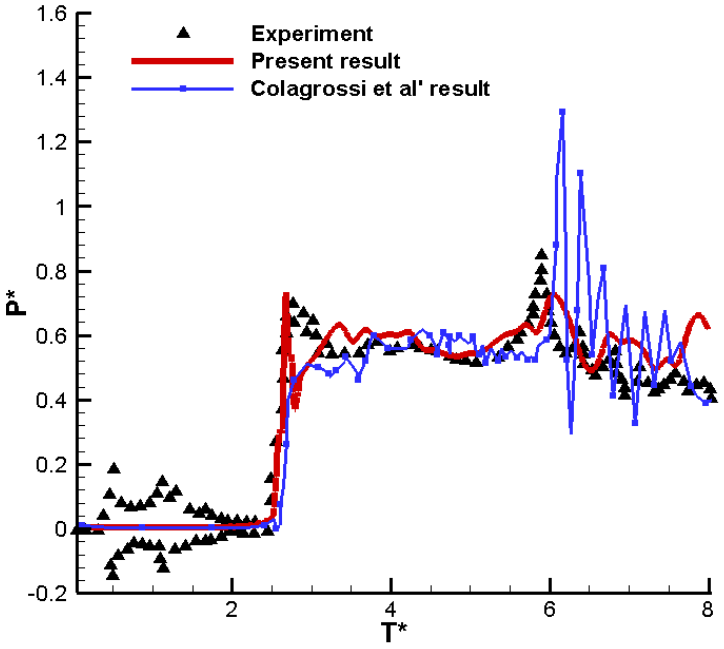

Fig. 3. Comparison of the time history of dimensionless pressure.
$P^* = (P - P_0)/(\rho_0 g h),\ T^* = t\sqrt{g/h}.$

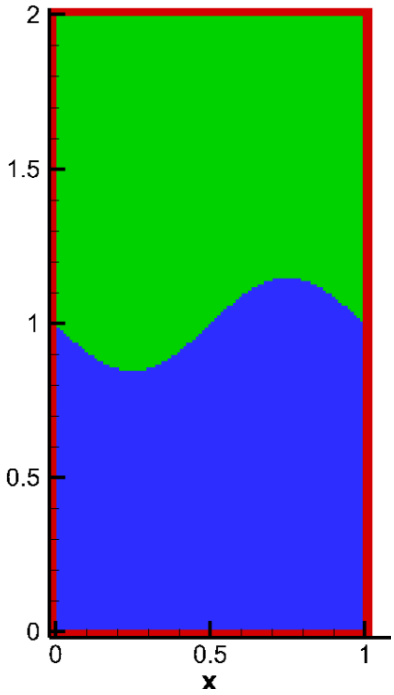

Fig .4. Initial setup of Rayleigh–Taylor instability.

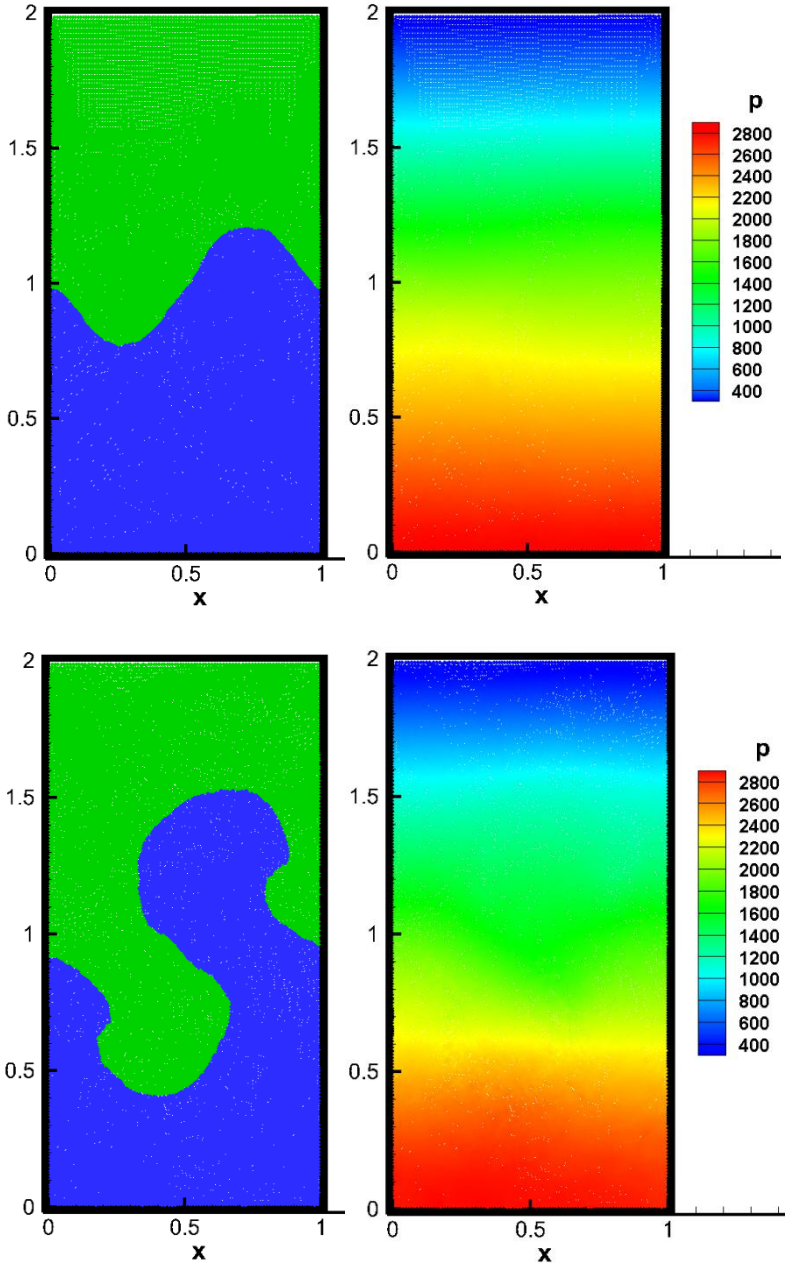

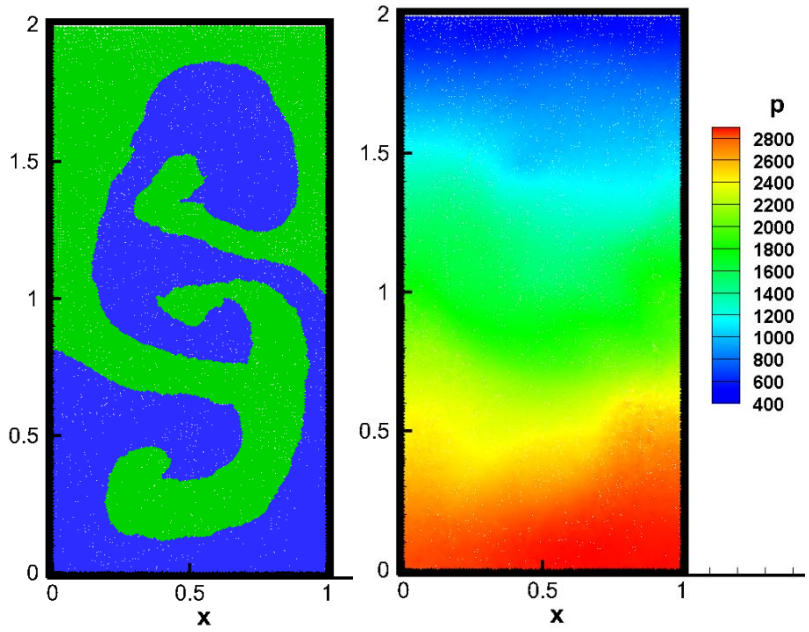

Fig. 5. Snapshots of Rayleigh–Taylor instability with $\mathrm{dx0} = 0.005\,m$, at $\mathrm{t} = 1\,s,\ 3\,s$ and $5\,s$ (from top to bottom): left: phase distribution; right: pressure field.

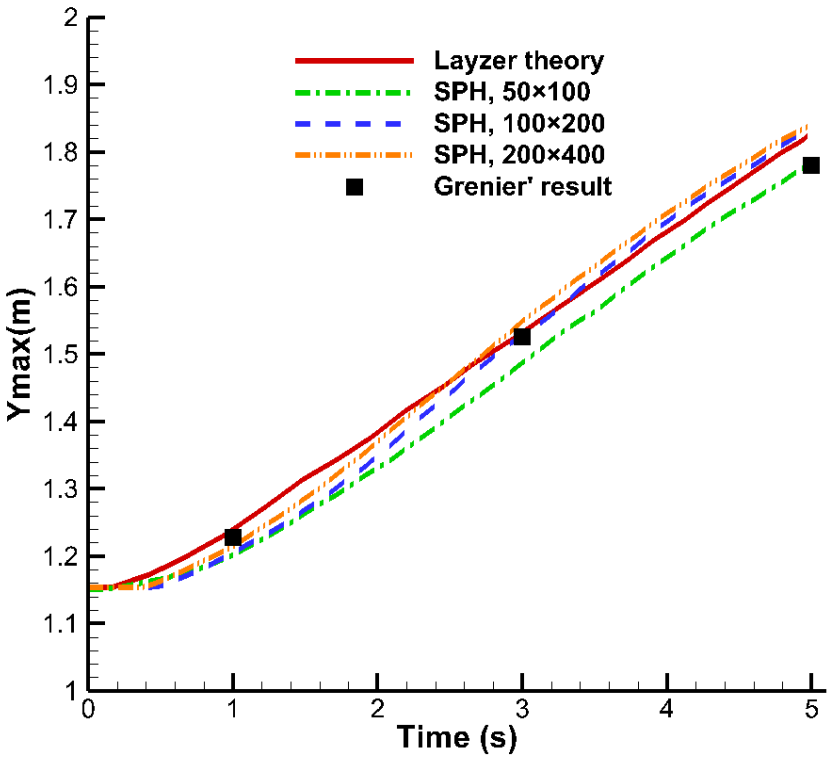

Fig. 6. The time variation of the highest point of the low-density fluid.

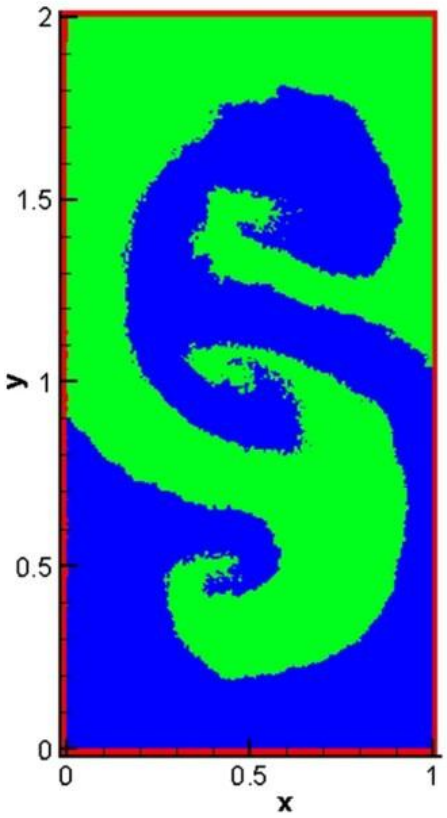

Fig. 7. Particle and phase distirubtion by Chen et al. [18] at $\mathrm{t} = 5\ s$..

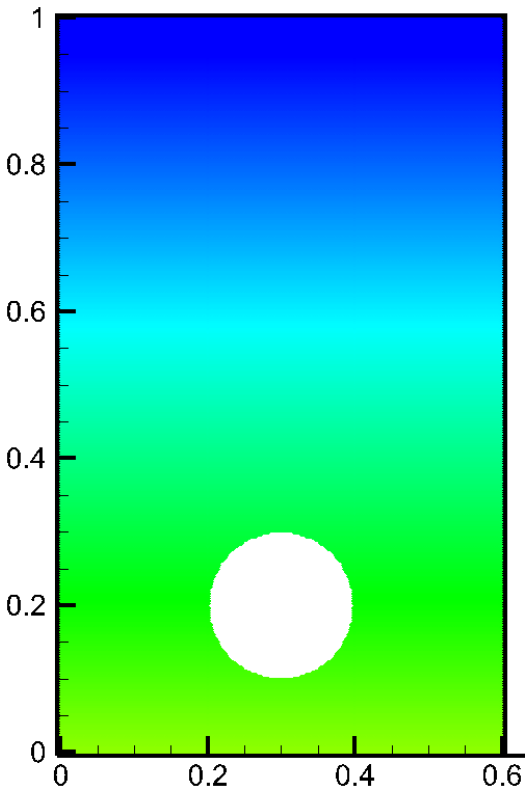

Fig. 8. The initial setup of the air bubble in a water tank.

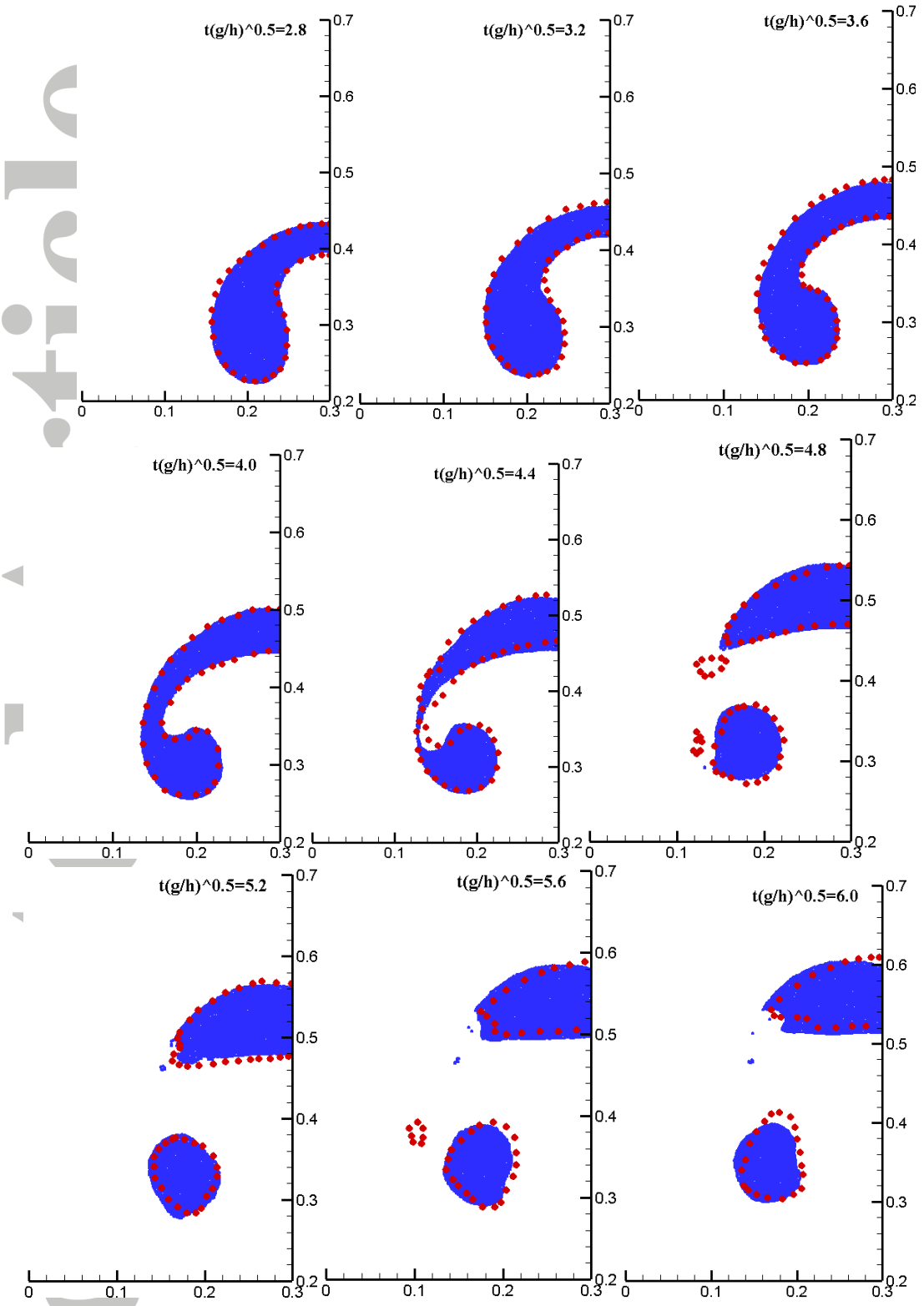

Fig. 9 Bubble shape evolution process together with the water-air interface (marked by red dots) obtained from Level-Set simulation [40].

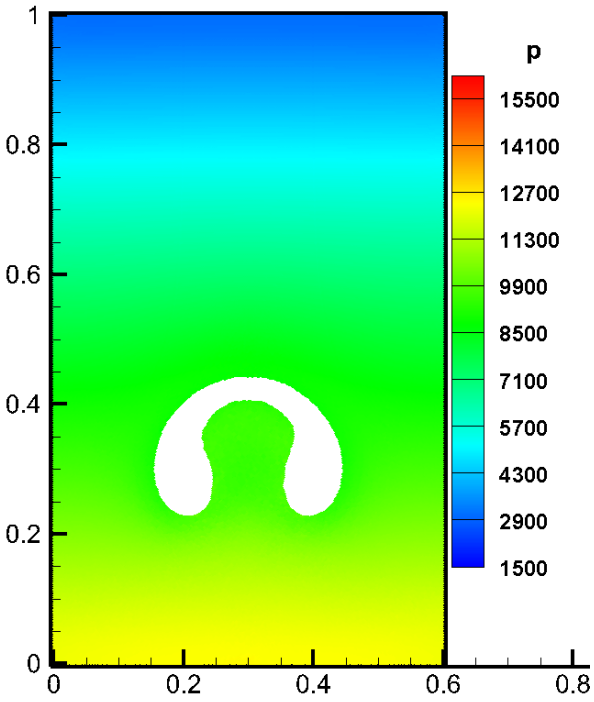

Fig. 10. Pressure field at t $\sqrt{(g/h)}$=3.0.

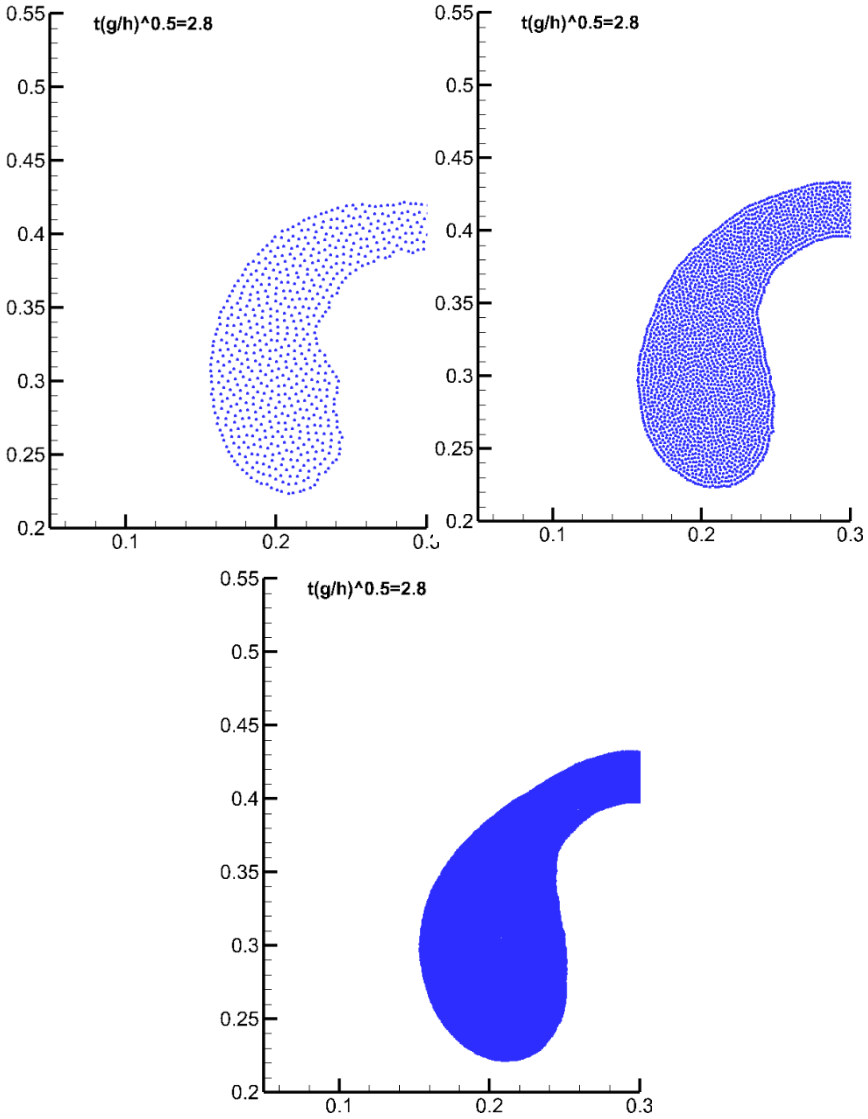

Fig. 11. Convergence study with the initial particle spacing from $\mathrm{dx0} = 0.05\,m$, $0.0025\,m$ to $0.00125\,m$ (from left to right).